JOURNAL OF SPACECRAFT AND ROCKETS
Vol. 39, No. 1, January–February 2002

# Graphical Method for Gravity-Assist Trajectory Design

Nathan J. Strange* and James M. Longuski†
*Purdue University, West Lafayette, Indiana 47907-1282*

**A new analytical technique directly related to Tisserand's criterion that permits the quick identification of all viable ballistic gravity-assist sequences to a given destination is introduced. The method is best presented by a simple graphical technique. The graphical technique readily demonstrates that gravity assists via Venus, Earth, and Jupiter are tremendously effective in sequences such as Venus–Earth–Earth–Jupiter and Venus–Earth–Mars–Earth. Estimates are made for the shortest flight times for a given launch energy to each planet. This graphical technique should provide mission designers with a potent tool for finding economical gravity-assist trajectories to many targets of high scientific interest in the solar system.**

## Nomenclature

| | | |
|---|---|---|
| $a$ | = | semimajor axis, astronomical units (AU) |
| $E$ | = | specific energy, km$^2$/s$^2$ |
| $e$ | = | eccentricity |
| $H$ | = | hyperbolic anomaly of the flyby, rad |
| $i$ | = | inclination, deg |
| $P$ | = | period, days |
| $r_p$ | = | periapsis distance, AU |
| $r_{\text{Planet}}$ | = | average distance from sun to planet, AU |
| $T$ | = | Tisserand invariant, dimensionless |
| $t$ | = | time from periapsis to the flyby, s |
| $V$ | = | heliocentric velocity of spacecraft, km/s |
| $V_{\text{Planet}}$ | = | heliocentric velocity of planet, km/s |
| $V_\infty$ | = | hyperbolic excess velocity, km/s |
| $X$ | = | eccentric anomaly of the flyby, rad |
| $\Delta V$ | = | change in velocity, km/s |
| $\mu$ | = | gravitational parameter of central body, km$^3$/s$^2$ |

*Subscripts*

| | | |
|---|---|---|
| 1 | = | flyby of the innermost planet on a leg of a tour |
| 2 | = | flyby of the outermost planet on a leg of a tour |

*Superscripts*

| | | |
|---|---|---|
| $-$ | = | quantity before flyby |
| $+$ | = | quantity after flyby |

## Introduction

MISSIONS to the outer solar system and to Mercury can be expensive in terms of both launch cost and travel time. The technique of gravity assist has been key to either lowering launch mass or flight time (or both) and, hence, to making accessible such targets of great scientific interest. Many highly successful missions, including Mariner 10, Pioneers 10 and 11, and Voyagers I and II, have used gravity assists for deep space exploration.

In the 1800s, the work of Leverrier (see Broucke[1]) and Tisserand (see Roy[2]) on the perturbations of the orbits of planets and comets laid the foundation for the gravity-assist technique. In the 1950s, Battin[3] proposed using a planetary gravity assist to return a spacecraft to Earth without the use of propellant. Later, several investigators[4–9] studied the potential of gravity-assist swingby maneuvers for planetary exploration.

Well-known classical paths such as the Venus–Earth–Earth gravity-assist (VEEGA) trajectory used by the Galileo spacecraft have proved very effective. Yet, it is unclear whether or in what situations a better path might exist. Nonclassical paths such as the Venus–Earth–Mars–Earth proposed by Petropoulos et al.[10] can sometimes exceed the VEEGA's performance.

In this paper, we use an energy-based method to investigate the potential and to establish the performance envelope of various gravity-assist paths. Currently this technique does not readily admit the possibility of a propulsive $\Delta V$ maneuver between gravity assists. It is well known that such maneuvers can create new trajectory options, but for the present we exclude $\Delta V$ gravity-assist trajectories from our analysis. Thus, in our energy-based method we address only patched-conic ballistic trajectories, but the technique is sufficiently potent to assess all such alternatives.

## Approach

The satellite tour design program (STOUR) is a software tool that was developed at the Jet Propulsion Laboratory for the Galileo mission tour design.[11] This program has been enhanced and extended at Purdue University to enable the automated design of gravity-assist tours in the solar system as well as the satellite system of Jupiter.[12–15] STOUR uses a patched-conic method to calculate all gravity-assist trajectories meeting specified requirements.

Given a path or sequence of gravity-assist bodies, STOUR can step through a range of launch dates to find all gravity-assist trajectories that follow the path. The searches can be computationally intense, sometimes requiring weeks of computer time for wide launch windows and multiple flyby paths. A path of gravity-assist bodies must be specified before an STOUR run is executed. Often, the computation time required renders an exhaustive search of all possible paths infeasible. What is needed is a method to identify the most promising paths before conducting an STOUR search. In addition, a method is needed to identify all viable paths. Ideally, we want a method that generates the best trajectory (in terms of low launch energy and short flight time) to a given planet for any given launch period.

We will refer to the problem of identifying a sequence of gravity-assist bodies and assessing the potential of that sequence or path as path finding. Similarly, we refer to the process of propagating that path with a tool such as STOUR as path solving.

## Graphical Method

The $P$–$r_p$ plot developed for the Europa orbiter mission design[16] offers a method for selecting a ballistic path of gravity-assist bodies for computation in STOUR. This plot is an energy-based method similar to that employed by Hollenbeck[9] and to the gravity-assist potential plots described by Petropoulos et al.[10] The $P$–$r_p$ graph

Received 23 January 2001; revision received 25 July 2001; accepted for publication 30 July 2001. 

*M.S. Candidate, School of Aeronautics and Astronautics; currently Member, Technical Staff, Navigation and Mission Design Section, Mail Stop 230-205, Jet Propulsion Laboratory, California Institute of Technology, 4800 Oak Grove Drive, Pasadena, CA 91109-8099; nathan.strange@jpl.nasa.gov. Member AIAA.

†Professor, School of Aeronautics and Astronautics, 1282 Grissom Hall; longuski@ecn.purdue.edu. Associate Fellow AIAA.

uses energy contours related to Tisserand's criterion (see Roy[2]) to illustrate gravity-assist trajectories. A literature search shows that similar plots of period vs periapsis are used in the study of Cassini's Saturn orbit insertion.[17] Also, Labunsky et al.[18] describe a graphical method that is very similar to the $P$–$r_p$ method for the study of orbital transfers and gravity-assist maneuvers.

Figure 1 illustrates the mechanism of a gravity assist. The spacecraft's orbit relative to a flyby planet is a hyperbola, and the spacecraft's velocity relative to the planet when it is infinitely far away is $V_\infty$ (the hyperbolic excess velocity). The net effect of the flyby is to rotate the $\boldsymbol{V}_\infty$ vector from the incoming $\boldsymbol{V}_\infty^-$ to the outgoing $\boldsymbol{V}_\infty^+$, without changing the magnitude. The spacecraft's orbit about the sun is determined by its heliocentric velocity, which, using the patched conic method, is found from the addition of the $\boldsymbol{V}_\infty$ vector (i.e., the velocity relative to the planet) to the planet's velocity as shown in Fig. 2. Here, $V^-$ is the heliocentric velocity before the flyby, and $V^+$ is the velocity after the flyby. When the $\boldsymbol{V}_\infty$ vectors have the same magnitude, but different directions, we obtain different heliocentric velocities from this vector addition and, hence, heliocentric orbits with different periods and periapses.

In Fig. 2, when the angle $\alpha$ is zero, the $\boldsymbol{V}_\infty$ vector is aligned with the planet's velocity vector ($V_{\text{Planet}}$) providing the highest energy heliocentric orbit for that $V_\infty$. This alignment corresponds to the flyby being at periapsis of the heliocentric orbit. When $\alpha$ is 180 deg, the $\boldsymbol{V}_\infty$ vector is opposite to the planet's velocity vector, and we have the lowest heliocentric energy possible with the flyby at aphelion.

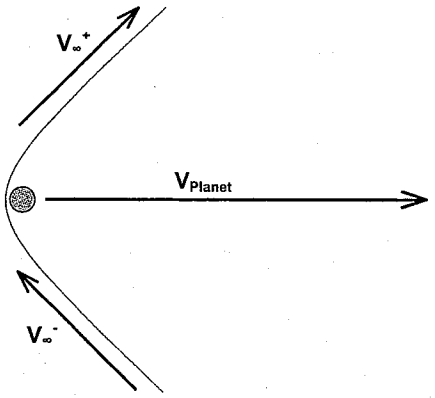


**Fig. 1 Gravity-assist schematic.**

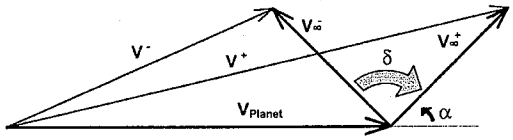


**Fig. 2 Gravity-assist vector diagram.**

Figure 3 shows a $P$–$r_p$ graph of heliocentric orbits in the ecliptic where we plot period $P$ vs periapsis $r_p$. A contour of orbits with a $V_\infty$ of 5 km/s with respect to Venus is shown. A gravity assist with Venus rotates the $\boldsymbol{V}_\infty$ vector of the spacecraft along this $V_\infty$ contour, modifying the orbit about the sun. A $V_\infty$ contour is the locus of orbits with the same energy relative to the planet. We note that a sequence of flybys with Venus may change the energy of a spacecraft relative to the sun and other planets, but not relative to Venus. In Fig. 3, the spacecraft values of $P$ and $r_p$ are confined to the one $V_\infty$ contour shown.

The farthest point to the upper right on the $V_\infty$ contour in Fig. 3 corresponds to positive alignment of the spacecraft's velocity vector with the planet's velocity ($\alpha = 0$ deg) and represents the highest heliocentric energy possible for encounter with the planet. Rotation of the $\boldsymbol{V}_\infty$ vector away from this alignment corresponds to moving from right to left on the $V_\infty$ contour toward negative alignment with the planet's velocity vector ($\alpha = 180$ deg). This point corresponds to the lowest heliocentric energy.

Venus's gravity determines how much a heliocentric orbit can be changed in one flyby without impacting the planet. We would like to constrain our flybys to a safe margin above the planet's surface, for example, 200 km. To indicate this altitude constraint, we use tick marks (shown as dots on the plot). From a given tick mark on a contour, the spacecraft's orbit may move a maximum distance indicated by the next tick mark (either up or down that contour) before violating the 200-km altitude constraint. When not starting at a tick mark, the nearby tick mark spacing can be used to estimate the distance the spacecraft may travel along the contour.

A $P$–$r_p$ plot combining several $V_\infty$ contours for Venus, Earth, Mars, and Jupiter is shown in Fig. 4. Here we assume that all of the planets are in circular and coplanar orbits. We also assume that the spacecraft is in the same plane as the planets. The contours in Fig. 4 start next to each planet's name at a $V_\infty$ of 1 km/s, then increase in steps of 2 km/s toward the upper left of the plot. Using tick marks, we constrain the flybys to a minimum altitude of 200 km at each terrestrial planet and to a minimum altitude of five Jovian radii at Jupiter.

The point where contours from different planets intersect represents a potential transfer orbit between those two planets. Comparing these contours gives the values of $V_\infty$ at each gravity-assist body for this transfer orbit. We can string together tours of the planets by connecting the contours, where the intersections indicate transfer orbits between each pair of planets in the tour. This process tells us whether a tour is possible from an energy standpoint but not from a phasing (timing) point of view, that is, we must assume that each

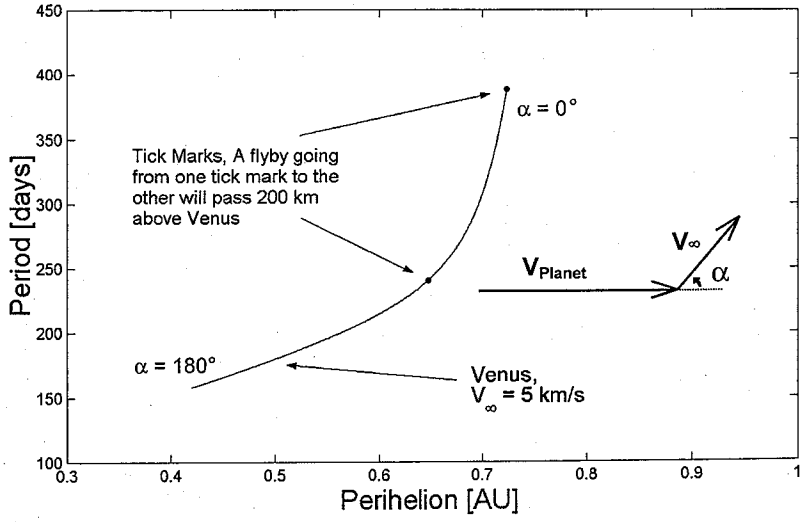


**Fig. 3 $V_\infty$ contour.**

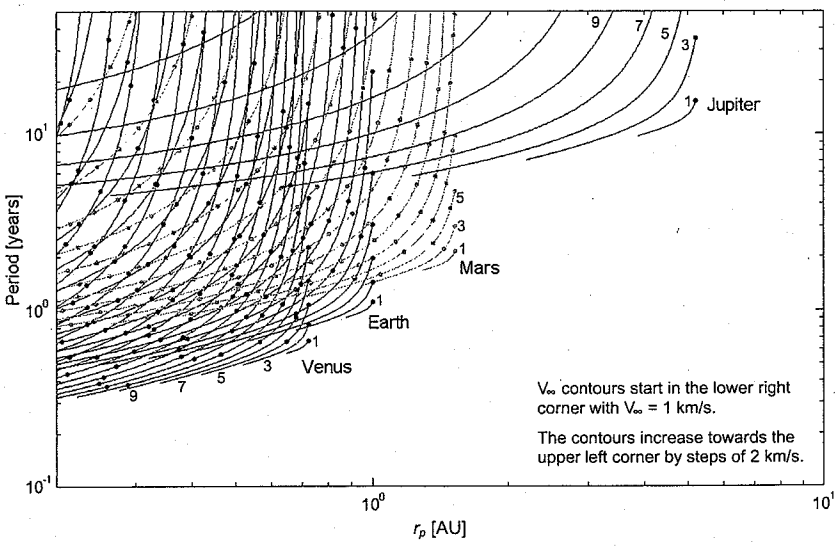


**Fig. 4 $P$–$r_p$ plot.**

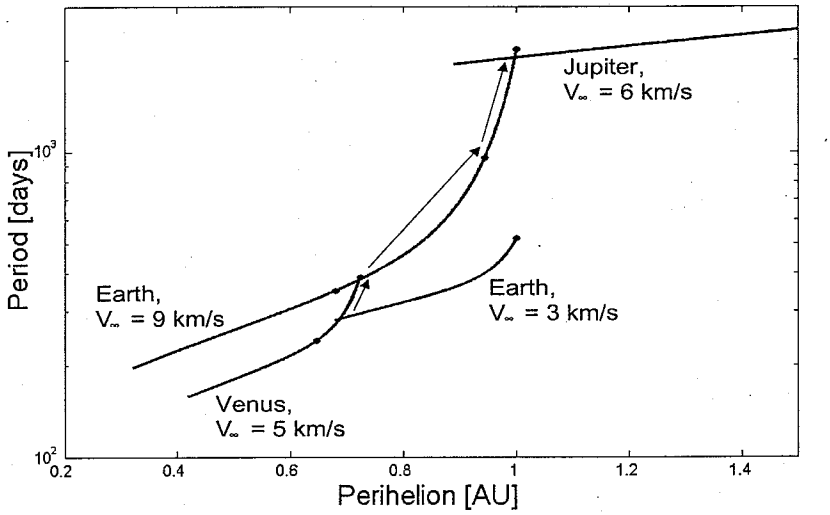


**Fig. 5 Illustrating a VEEGA with a $P$-$r_p$ plot.**

planet is always located at the proper position for the flyby to take place. In this way, we can assess the potential performance of a tour before the laborious calculations in a path-solving tool such as STOUR (which solves the phasing problem).

A $P$–$r_p$ plot can be used to easily find and evaluate paths for gravity-assist trajectories such as the VEEGA (Fig. 5). The VEEGA allows a low Earth launch energy (for this case, $V_\infty = 3$ km/s) to place a spacecraft on a Jupiter-bound trajectory. The VEEGA starts by launching into an orbit with a perihelion low enough to reach Venus. A single Venus flyby is then used to increase the spacecraft's $V_\infty$ at Earth to a value high enough to reach Jupiter, that is, 9 km/s. Two Earth flybys are then needed to rotate the spacecraft's $V_\infty$ vector so that it reaches Jupiter. (The distance to Jupiter along Earth's $V_\infty = 9$ km/s contour is greater than the tick mark spacing for one flyby, but less than the spacing of two tick marks. Thus, we know that two Earth flybys are required.) We see that the last leg of a VEEGA is effectively the same as launching from Earth with a higher energy ($V_\infty = 9$ vs 3 km/s).

In 1889, Tisserand discovered an invariant quantity that held for comets before and after perturbations of their orbits by Jupiter. He used this criterion to identify a comet with a new orbital period and perihelion as the same comet observed at an earlier date. The contours on the $P$–$r_p$ plot also represent orbits with the same Tisserand constant. Here we are using planets to intentionally perturb the spacecraft's orbit about the sun. Tisserand's criterion has long been used as a check of the assumptions made in designing trajectories with patched-conic analysis.[19] This invariant is given by

$$T = r_{\text{Planet}}/a + 2\left[a(1-e^2)/r_{\text{Planet}}\right]^{\frac{1}{2}} \cos i \qquad (1)$$

A plot of period vs periapsis can only depict elliptic and circular orbits. However, if we change the vertical axis from period to specific energy, we get another graph that can show hyperbolic and parabolic orbits as well. This $E$–$r_p$ plot can then represent all heliocentric orbits. Henceforth, we will formally refer to these graphs (both $P$–$r_p$ and $E$–$r_p$ plots) as Tisserand graphs in honor of the astronomer. Because we are assuming the planets to be in circular, coplanar orbits, the argument of periapsis and longitude of the ascending node of the heliocentric orbit have no effect on $V_\infty$ and flight-path angle. If we wish to consider spacecraft orbits outside of the ecliptic, we would add inclination as a third axis on these graphs, and our $V_\infty$ contours would become surfaces.

The relative scaling of the energies and distances of the inner planets in comparison to the outer planets makes generation of one readable Tisserand ($E$–$r_p$) graph impractical for the entire solar

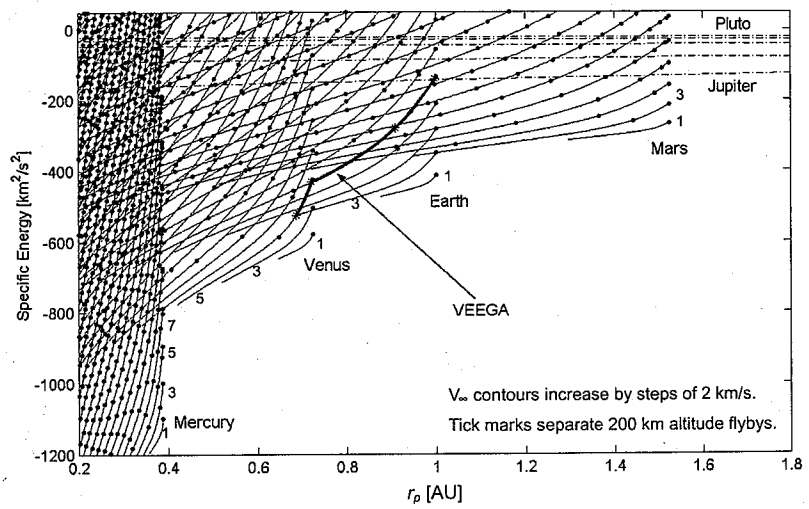


**Fig. 6 $E$–$r_p$ plot for the inner planets.**

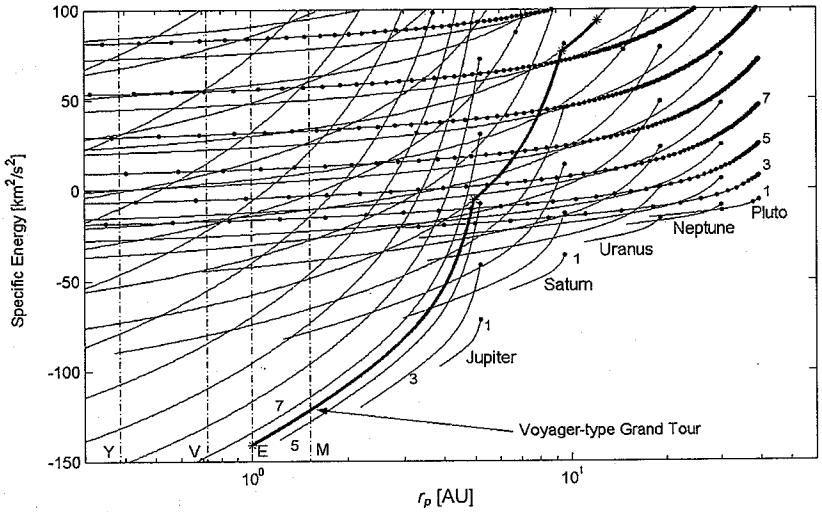


**Fig. 7 $E$–$r_p$ plot for the outer planets.**

system. It is more convenient to group the inner planets and outer planets separately as in Figs. 6 and 7. Figure 6 shows horizontal dash–dot lines for the energies of orbits that are able to reach each of the outer planets. Contours that cross the line labeled Jupiter are able to reach Jupiter, contours that cross the next line may reach Saturn, etc. A VEEGA path reaching Jupiter is illustrated on this plot. The $V_\infty$ contours start at 1 km/s and increase in steps of 2 km/s toward the upper left of the plot. The tick mark spacings indicate the 200-km altitude constraint for the terrestrial planets.

Figure 7 shows vertical dash–dotted lines for orbits with periapses that can reach the various inner planets (where Y stands for Mercury, V for Venus, E for Earth, and M for Mars). A Voyager-type grand tour path starting from Earth is shown. On this plot the $V_\infty$ contours also start at 1 km/s and increase toward the upper left by steps of 2 km/s. However, the tick mark spacing is different for each planet. Jupiter's (altitude) tick marks are spaced at five Jovian radii to mitigate radiation. Saturn's tick marks are spaced at an altitude of two Saturnian radii to avoid the rings. Uranus's and Neptune's tick marks are spaced by one planetary radii to avoid rings as well, and Pluto's tick marks are spaced for the 200-km constraint.

Although these two Tisserand graphs can be used in combination to design tours, it is often much easier to generate a new plot with only the four or five planets of interest for the tour. For example, a useful Tisserand graph often includes the destination planet and Venus, Earth, Mars, and sometimes Jupiter.

Figure 8 shows a plot to design tours to Mercury with $V_\infty$ contours incremented by steps of 2 km/s. Two paths are shown launching from Earth with a $V_\infty$ of 3 km/s. One path is Earth–Venus–Earth–Mercury (EVEY) and arrives at Mercury with a $V_\infty$ of 12 km/s (this value is interpolated between the 11 and 13 km/s Mercury $V_\infty$ contours). The second path is EVEVY, which arrives at 11 km/s.

Figure 9 shows $V_\infty$ contours for Venus, Earth, Mars, and Jupiter for missions to the outer planets. For a launch of $V_\infty = 3$ km/s, we can identify several paths that get to Jupiter: EVEEJ, EVEMEJ, EVEVEJ, EVEEMJ, EVEVVVJ, EMEMEEJ, etc. In addition, we can see that once any trajectory gets to Jupiter from Earth or Venus, it can reach any of the outer planets by a single Jupiter gravity assist.

If we start with the simplest of the Jupiter trajectories, the VEEGA, we can increase its effectiveness by adding a $V_\infty$-leveraging flyby with Mars or Venus between the two gravity assists. Although Mars has closer tick marks than Venus, that is, it has less gravity, a $V_\infty$-leveraging flyby of Mars moves the spacecraft farther up the Earth $V_\infty$ contours, enabling it to achieve a higher final heliocentric energy than with Venus as a $V_\infty$-leveraging body. We can also see cases where pumping down i.e., decreasing heliocentric energy, at Mars gives a larger $V_\infty$ at Venus or Earth, which can then deliver a spacecraft to Jupiter, whereas with two or three Mars pump-ups, i.e., flybys that increase heliocentric energy, the spacecraft could not reach Jupiter.

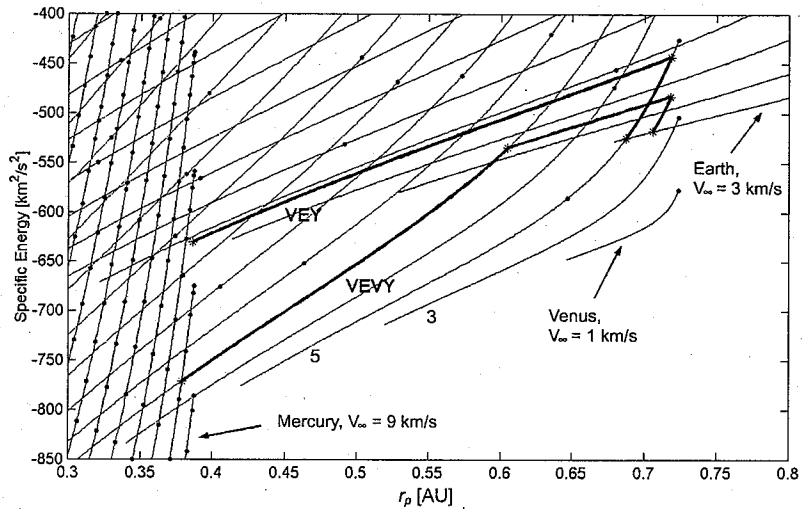


**Fig. 8 Mercury $E$–$r_p$ plot.**

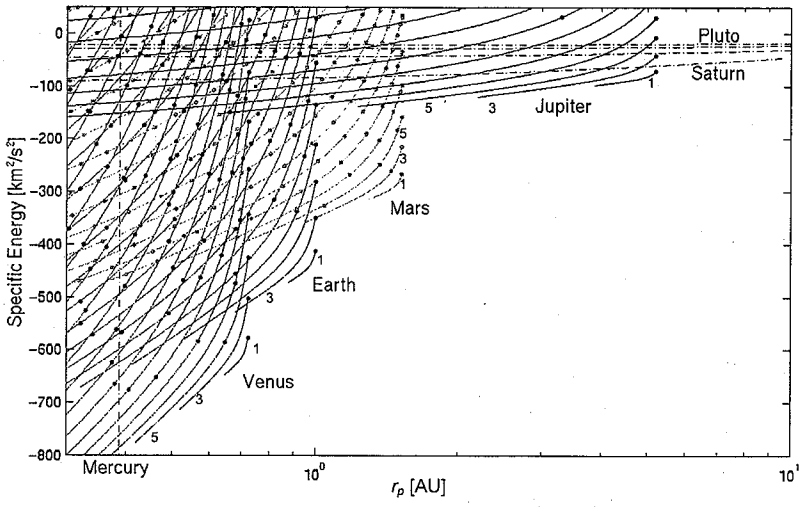


**Fig. 9 $E$–$r_p$ design plot.**

By generating these plots for a specific problem, we can easily determine the minimum launch energy to fly a given path, or the minimum number of flyby bodies needed to reach a destination for a given launch energy. However, we would also like to compare the flight times for different paths. For example, we would like to know if a high-energy five-body path is faster or slower than a low-energy three-body path.

## Flight Time

Flight time can be estimated for a path found by our graphical method. Given the periapsis and specific energy of the transfer orbit, there is a finite set of arcs that connect the two planets on the transfer orbit. If we limit our consideration to orbits that complete less than one revolution about the sun, then there are eight arcs that connect two planets for a given periapsis and energy.

A point where two $V_\infty$ contours intersect is an orbit that crosses the orbits of two planets. This orbit can be used to travel from the planet nearer the sun to the planet further out, that is, "up." The orbit can also be used to travel from the outermost planet to the planet closer to the sun, or "down." Additionally, each of the two planetary encounters may be on either an outbound, that is, after periapsis and before apoapsis, or an inbound, that is, before periapsis, leg. The eight permutations of these possibilities give rise to eight possible transfer arcs between two planets for a given specific energy and periapsis (ignoring multiple revolutions).

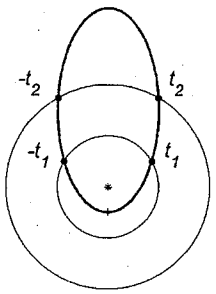


**Fig. 10 Possible (counterclockwise) transfer arcs.**

Figure 10 illustrates the possible transfers. In Fig. 10, $t_1$ is the time from periapsis of the transfer orbit to its crossing of the inner planet's orbit, and $t_2$ is time to its crossing of the outer planet's orbit. Here, an up transfer that leaves the innermost planet outbound and arrives at the second planet outbound goes from $t_1$ to $t_2$. Similarly, a transfer from $-t_2$ to $t_1$ would be a down transfer leaving inbound and arriving outbound, where $t_1$ and $t_2$ are positive.

Table 1 shows the flight time for these permutations. In Table 1, I–I denotes a transfer leaving the first planet inbound and arriving at the second planet inbound, O–I leaves the first planet outbound and arrives at the second inbound, etc. Here, $P$ is the period of the

**Table 1 Flight times for possible arcs**

| Up[a] | Down[b] | Flight time |
|---|---|---|
| I–I | O–O | $P + t_1 - t_2$[c] |
| O–I | O–I | $P - t_1 - t_2$[c] |
| I–O | I–O | $t_1 + t_2$ |
| O–O | I–I | $t_2 - t_1$ |

[a]Up denotes transfers ending farther from the sun.
[b]Down denotes transfers ending nearer the sun.
[c]This arc is not possible for hyperbolic or parabolic orbits because it requires flying through apoapsis.

orbit, $t_1$ is the time from periapsis of the orbit at the inner planet encounter, and $t_2$ is the time for the outer planet encounter. The first two rows in Table 1 are for elliptic arcs only because they require flying through apoapsis. The positive times used in Fig. 10 and Table 1 are computed from Kepler's equations:

$$t_1 = |(P/2\pi)[X_1 - e\sin(X_1)]| \tag{2}$$

$$t_2 = |\sqrt{(a^3/\mu)}[e\sinh(H_1) - H_1]| \tag{3}$$

where Eq. (2) applies to elliptic transfers, Eq. (3) applies to hyperbolic transfers, $X_1$ is the eccentric anomaly of the inner planet flyby, and $H_1$ is the hyperbolic anomaly. These equations provide $t_1$; to obtain $t_2$ the appropriate eccentric anomaly $X_2$ or hyperbolic anomaly $H_2$ is substituted for the outer planet's flyby.

When stringing these arcs together for a path, we must take care that when the spacecraft arrives at a planet inbound that it also leaves the planet inbound. Similarly, when the spacecraft arrives outbound it also leaves outbound. The one exception is when we are able to overturn the velocity vector to get the same heliocentric flight-path angle, but inbound rather than outbound (or vice versa). This exception happens at the far left and far right ends of a $V_\infty$ contour when there is enough turning to go all of the way to the end; further turning reverses the direction of travel on the $V_\infty$ contour (the spacecraft comes back down the contour with the opposite heliocentric flight-path angle).

The time of flight estimate is calculated by a MATLAB® script, using the algorithm (discussed later) to connect contours on a plot into tours. This program selects the minimum time (hypothetically) possible to get to a given planet for a given launch energy. The phasing (timing) problem is ignored in these calculations, and so the results can range from optimistic to infeasible.

## Automated Traversal of Tisserand Graphs

To search automatically for possible tours on a Tisserand graph, the plot is discretized. We do this by selecting a set of $V_\infty$ contours for each planet. Where these contours intersect is a node of the grid and a possible transfer orbit for a tour. Additional nodes are added for resonant orbits at each planet.

Traversal of the graph begins by choosing a set of nodes on a launch $V_\infty$ contour. Then we construct a second level of nodes from all nodes that can be reached in a single flyby from our starting set of nodes. The flight time from each initial node to each node on the second level is calculated, and the fastest flight time (and the initial node for that flight time) is saved for each node on the second level. This step gives us the first two flyby bodies in paths to each node on the second level.

After the fastest path to each node on the second level has been computed, we construct a third level comprising all nodes that can be reached by one flyby from the nodes on the second level. Again, we save the fastest flight time to each node on the third, along with the initial node and the node on the second level, thus building a path to the node on the third level. This process continues across the grid until the fastest path to every node on the grid is computed. If, from the third level or higher it is possible to reach a node on the second level faster than from the first, the faster path is used and that node is then moved up to the fourth level or higher (based on how many flybys are needed in the path to get that low cost).

An added complexity to the process is that the flight time from one node to another depends on whether the spacecraft encounters each planet inbound or outbound and whether it is going up or down (see Fig. 10 and Table 1). To account for the different types of encounters, two cost functions are tracked for each node. One is the time of flight for a path whose final flyby is outbound, the other inbound.

This algorithm finds the fastest path to every planet on the grid for discrete values of $V_\infty$. The fastest path for a specified arrival $V_\infty$ contour is also calculated. Visual inspection of a Tisserand graph already tells us the minimum number of flyby bodies to reach a planet or if a given path can even reach a planet. For a destination planet and a launch $V_\infty$ contour, this algorithm can predict the fastest path to that planet from an energy basis. However, the required location of the planets, that is, the phasing required to fly this path, may occur rarely or never.

## Results

Table 2 shows the potentially fastest path to each of the nine planets for launch $V_\infty$ values of 3, 5, 7, 9, and 11 km/s (ignoring phasing). Table 2 was generated on a grid of $V_\infty$ contours separated by 1 km/s. Paths are truncated after the fifth body. (When no limit on flybys is imposed, we find 15- and 17-body paths to Pluto with infeasible phasing.) The lowest Hohmann $V_\infty$ is used as the lower bound for each planet's contours in constructing the grid; the upper bound is set based on the most energetic heliocentric hyperbola that can be created with gravity assists. Resonant orbits of up to 6:1 (i.e., six planet revolutions to one spacecraft revolution) are considered for all of the inner planets (Y, V, E, and M). For Earth, Venus, and Mars the resonances: 3:2, 1:2, and 1:3 are considered as well. Additional nodes are incorporated with the correct orbit periods for these resonant transfers.

Table 2 should be interpreted as a performance envelope of the flight time needed for a given launch energy. This analysis assumes that the planets are in the correct position for the best flyby (in terms

**Table 2 Potentially fastest paths (ignoring phasing)**

| Launch $V_\infty$, km/s | Path | Flight time, years |
|---|---|---|
| 3 | EVEVY | 0.8 |
| 3 | EV | 0.3 |
| 3 | EVEM | 0.7 |
| 3 | EVEVEJ | 2.4 |
| 3 | EVEEJS | 7.5 |
| 3 | EVEEJU | 13.0 |
| 3 | EVEEJN | 20.0 |
| 3 | EVEEJP | 27.8 |
| 5 | EVY | 0.3 |
| 5 | EV | 0.2 |
| 5 | EM | 0.3 |
| 5 | EVEVEJ | 2.1 |
| 5 | EVMVES | 4.2 |
| 5 | EVEMJU | 8.1 |
| 5 | EVEEJN | 11.3 |
| 5 | EVEEJP | 13.7 |
| 7 | EVY | 0.2 |
| 7 | EV | 0.1 |
| 7 | EM | 0.3 |
| 7 | EMEMJ | 2.0 |
| 7 | EMEMJS | 3.7 |
| 7 | EMEMJU | 6.6 |
| 7 | EMEJSN | 9.9 |
| 7 | EMSJSP[a] | 12.3 |
| 9 | EVY | 0.2 |
| 9 | EV | 0.1 |
| 9 | EM | 0.2 |
| 9 | EMEJ | 1.7 |
| 9 | EMEJS | 3.1 |
| 9 | EMEJSU | 5.5 |
| 9 | EMEJSN | 7.9 |
| 9 | EMEJSP | 9.9 |
| 11 | EVY | 0.2 |
| 11 | EV | 0.1 |
| 11 | EM | 0.2 |
| 11 | EMJ | 1.3 |
| 11 | EMJS | 2.6 |
| 11 | EMEJSU | 4.7 |
| 11 | EMEJSN | 6.9 |
| 11 | EMEJSP | 8.7 |

[a]This path is not possible due to the phasing of two Saturn flybys.

**Table 3 Flight times for potential gravity-assist paths (ignoring phasing)**

| Path[a] | Launch $V_\infty$, km/s | Jupiter, years | Saturn, years | Uranus, years | Neptune, years | Pluto, years |
|---|---|---|---|---|---|---|
| EVEX | 6 | 2.3 | N/T[b] | N/T | N/T | N/T |
| EVEEX | 3 | 4.8 | N/T | N/T | N/T | N/T |
| EVEEX | 4 | 3.9 | 6.8 | 13.6 | N/T | N/T |
| EVEEX | 5 | 3.8 | 6.5 | 12.4 | 19.0 | 25.8 |
| EVEEX | 7 | 3.8 | 6.5 | 12.4 | 19.0 | 25.8 |
| EVVVX | 6 | 5.8 | N/T | N/T | N/T | N/T |
| EVEMX | 5 | 2.2 | N/T | N/T | N/T | N/T |
| EVEEMX | 5 | 3.8 | 6.3 | 11.9 | 19.5 | 27.5 |
| EVEVEX | 3 | 2.4 | N/T | N/T | N/T | N/T |
| EVEVEX | 5 | 2.1 | 5.0 | N/T | N/T | N/T |
| EVEMEX | 3 | 2.7 | N/T | N/T | N/T | N/T |
| EVEMEX | 5 | 3.3 | 6.7 | 12.0 | 20.2 | 28.2 |
| EVEVEEX | 3 | 4.2 | 6.9 | 12.7 | 18.2 | 23.5 |
| EVEMEEX | 3 | 4.7 | 8.0 | 14.8 | N/T | N/T |
| | | *Paths with Jovian gravity assist* | | | | |
| EJX | 9 | — | 5.0 | 10.4 | 17.4 | 25.3 |
| EJX | 11 | — | 2.7 | 5.4 | 8.4 | 11.0 |
| EVEJX | 6 | — | 4.7 | 9.2 | 14.8 | 20.8 |
| EVVVJX | 6 | — | 7.9 | 11.7 | 16.0 | 19.5 |
| EVEEJX | 3 | — | 7.5 | 13.0 | 20.0 | 27.8 |
| EVEEJX | 5 | — | 5.5 | 8.5 | 11.3 | 13.7 |
| EVEEJX | 9 | — | 5.4 | 8.4 | 11.2 | 13.7 |
| EVEVEJX | 3 | — | 4.4 | 7.9 | 12.2 | 15.7 |
| EVEVEJX | 5 | — | 3.5 | 6.2 | 9.2 | 11.7 |

[a]Where X represents the terminal planet in the path, that is, Jupiter, Saturn, Uranus, Neptune, or Pluto.
[b]No trajectory exists to this destination planet for this path and launch energy.

of flight time) and, as such, probably underestimates the flight time required for most paths. Furthermore, paths containing sequences such as VMV or MEM may never occur due to the requirement that a planet be in the proper position for a second flyby. Clearly, the path EMSJSP for the launch $V_\infty$ of 7 km/s is infeasible for this reason.

Table 3 shows flight times to the outer planets for a sampling of paths at various launch energies. We notice that paths such as VEEGA perform very well for low launch energies but begin to offer diminishing returns as we increase launch energy; an increase of launch $V_\infty$ from 5 to 7 km/s offers no significant improvement. Our preliminary investigation with the path-solving tool STOUR shows that these flight time estimates tend to be roughly 30% below what STOUR finds for the next 40 years. Petropoulos et al.[10] found all paths to Jupiter given in Table 3 for launch opportunities in 1999–2030, with the exception of the EVEVEE and EVEMEE paths, which they did not investigate.

Tables 1–3 can be used in conjunction with the Tisserand graphs to give a ballpark estimate of the flight time for different paths. However a path solving tool is needed to account for phasing. The program STOUR solves not only the phasing problem, but also provides for three-dimensional transfers between noncircular, noncoplanar planetary orbits.

Our method has application beyond the design of purely ballistic trajectories. For example, Johnson and Longuski[20] use Tisserand graphs to assess the performance of aerogravity-assist trajectories. Future work may include the analysis of deterministic trajectory maneuvers between gravity assists such as in $\Delta V$-Earth gravity-assist trajectories.

## Conclusions

Tisserand graphs facilitate the assessment of potential gravity-assist paths comprising purely ballistic transfer legs. Both arrival and launch $V_\infty$ may be studied for such a path. The graphs also make many characteristics of a possible path highly conspicuous.

Tisserand graphs are a powerful tool that permits us to readily construct gravity-assist paths to any destination in the solar system. All paths so constructed are feasible from an energy perspective. Paths that do not exist on a Tisserand graph are strictly infeasible for ballistic trajectories. Thus, we can eliminate unnecessary searches and confine path finding to those that obey the criterion. Estimates of flight time can be made for a given launch $V_\infty$, thus providing another criterion for candidate rejection. After applying these criteria, the mission designer can be assured that the remaining candidate paths found are worth pursuing in the laborious calculation that must follow to solve the phasing problem. This last problem, path solving, is well known and discussed in great detail in the literature.

## Acknowledgments

This research has been supported in part by the Jet Propulsion Laboratory (JPL), California Institute of Technology, under Contract 1211514 (Gregory T. Rosalia, Contract Manager and Dennis V. Byrnes, Technical Manager). We thank Andrew F. Heaton, Wyatt R. Johnson, and Anastassios E. Petropoulos for their assistance in developing some of the techniques described in this paper. We also thank Daniel J. Scheeres for pointing out the connection of our graphical technique to Tisserand's criterion. Finally, we thank Louis A. D'Amario, Eugene P. Bonfiglio, Dennis V. Byrnes, Jennie R. Johannesen, and Jan M. Ludwinski at JPL for their generous support, enthusiastic collaboration, and expert guidance with regard to the Europa orbiter mission, which inspired these techniques.

## References

[1]Broucke, R. A., "The Celestial Mechanics of Gravity Assist," AIAA Paper 88-4220, Aug. 1988.

[2]Roy, A. E., *Orbital Motion*, 2nd ed., Adam Hilger, Bristol, England, U.K., 1982, pp. 129–130.

[3]Battin, R. H., "The Determination of Round-Trip Planetary Reconnaissance Trajectories," *Journal of the Aero/Space Sciences*, Vol. 26, No. 9, 1959, pp. 545–567.

[4]Sedov, L. I., "Orbits of Cosmic Rockets Toward the Moon," *ARS Journal*, Vol. 30, No. 1, 1960, pp. 14–21.

[5]Minovitch, M. A., "The Determination of Characteristics of Ballistic Interplanetary Trajectories Under the Influence of Multiple Planetary Attractions," Jet Propulsion Lab., TR 32-464, California Inst. of Technology, Pasadena, CA, Oct. 1963.

[6]Deerwester, J. M., "Jupiter Swingby Missions to the Outer Planets," *Journal of Spacecraft and Rockets*, Vol. 3, No. 10, 1966, pp. 1564–1567.

[7]Flandro, G. A., "Fast Reconnaissance Missions to the Outer Solar System Utilizing Energy Derived from the Gravitational Filed of Jupiter," *Astronautica Acta*, Vol. 12, No. 4, 1966, pp. 329–337.

[8]Farquhar, R., and Stern, S. A., "Pushing Back the Frontier: A Mission to the Pluto–Charon System," *Planetary Report*, Vol. 10, No. 4, 1990, pp. 18–23.

[9]Hollenbeck, G. R., "New Flight Techniques for Outer Planet Missions," American Astronautical Society, AAS Paper 75-087, July 1975.

[10]Petropoulos, A. E., Longuski, J. M., and Bonfiglio, E. P., "Trajectories to Jupiter via Gravity Assists from Venus, Earth, and Mars," *Journal of Spacecraft and Rockets*, Vol. 37, No. 6, 2000, pp. 776–783.

[11]Rinderle, E. A., "Galileo User's Guide, Mission Design System, Satellite Tour Analysis and Design Subsystem," Jet Propulsion Lab., Rept. JPL D-263, California Inst. of Technology, Pasadena, CA, July 1986.

[12]Williams, S. N., "Automated Design of Multiple Encounter Gravity-Assist Trajectories," M.S. Thesis, School of Aeronautics and Astronautics, Purdue Univ., West Lafayette, IN, Aug. 1990.

[13]Longuski, J. M., and Williams, S. N., "Automated Design of Gravity-Assist Trajectories to Mars and the Outer Planets," *Celestial Mechanics and Dynamical Astronomy*, Vol. 52, No. 3, 1991, pp. 207–220.

[14]Patel, M. R., "Automated Design of Delta-V Gravity-Assist Trajectories for Solar System Exploration," M.S. Thesis, School of Aeronautics and Astronautics, Purdue Univ., West Lafayette, IN, Aug. 1993.

[15]Bonfiglio, E. P., "Automated Design of Gravity-Assist and Aerogravity-Assist Trajectories," M.S. Thesis, School of Aeronautics and Astronautics, Purdue Univ., West Lafayette, IN, Aug. 1999.

[16]Heaton, A. F., Strange, N. J., Longuski, J. M., and Bonfiglio, E. B., "Automated Design of the Europa Orbiter Tour," *Journal of Spacecraft and Rockets*, Vol. 39, No. 1, 2002, pp. 17–22; also AIAA Paper 2000-4034, Aug. 2000.

[17]Weinstein, S. S., and Stetson, D. S., "Saturn Orbit Insertion Options for the Cassini Mission," American Astronautical Society, AAS Paper 89-433, Aug. 1989.

[18]Labunsky, A. V., Papkov, O. V., Sukhanov, K. G., *Multiple Gravity Assist Interplanetary Trajectories*, Gordon and Breach Science Publishers, Newark, NJ, 1998, pp. 33–54.

[19]Szebehely, V., *Theory of Orbits: The Restricted Problem of Three Bodies*, Academic Press, New York, 1967, pp. 586, 587.

[20]Johnson, W. R., and Longuski, J. M., "Design of Aerogravity-Assist Trajectories," *Journal of Spacecraft and Rockets*, Vol. 39, No. 1, 2002, pp. 23–30; also AIAA Paper 2000-4031, Aug. 2000.

C. A. Kluever
*Associate Editor*